

## REPORT ON RADON EMISSIONS FROM SOIL AND RADON IN OUTDOOR AIR AT WOOMERA AREA

*Sylvester Werczynski*  
*October, 2018*

Measurements of emissions from soil of radon-222 (radon) and radon-220 (thoron) as well as ambient air radon have been performed at the Woomera Defence site between end of May and beginning of September 2018 as part of the baseline monitoring of the site and to measure potential occupational radiological exposures. Soil emissions were measured using a portable accumulation chamber, and radon in air measured using a dual-flow-loop two-filter radon detector (Whittlestone and Zahorowski<sup>1</sup>, 1998; Chambers et al., 2011<sup>2</sup>).

During the week of 29<sup>th</sup> -31<sup>st</sup> May 2018, 18 different locations on the site of interest were selected for spot measurements of radon emissions from soil. In addition, a 100L detector was set up on the southern side of the survey area to monitor radon concentrations continuously with a time resolution of 1 hour.

### Radon flux survey

In order to characterise the surface radon emissions from soil at the area of interest, the ANSTO radon emanometer<sup>3</sup> was used. The instrument is designed to simultaneously measure the radon and thoron flux densities from soil or rock surfaces. Radon and thoron flux estimates are made based on the flow-through accumulator method, with each sample taking approximately 24 minutes.

The strength of radon emissions from the land surface into the atmosphere depends on the soil mineralogy and porosity, and to a lesser extent also varies with changes in atmospheric pressure and soil moisture. Roughly speaking, the instantaneous flux should be within around a factor of two of the long term mean<sup>4</sup>.

The ANSTO portable accumulation chamber allows radon to accumulate in a chamber placed over the soil. The evolution of the measured radon concentration within the chamber is continuously monitored, and the surface flux at that location can then be estimated from the accumulation rate.

---

<sup>1</sup> Whittlestone, S. and Zahorowski, W.: Baseline radon detectors for shipboard use: development and deployment in the First Aerosol Characterization Experiment (ACE 1), *J. Geophys. Res.*, 103, 16743–16751, doi:10.1029/98JD00687, 1998.

<sup>2</sup> Chambers, S., Williams, A. G., Zahorowski, W., Griffiths, A., and Crawford, J.: Separating remote fetch and local mixing influences on vertical radon measurements in the lower atmosphere, *Tellus B*, 63, 843–859, doi:10.1111/j.1600-0889.2011.00565.x, 2011.

<sup>3</sup> Zahorowski, W. and Whittlestone, S.: A Fast Portable Emanometer for Field Measurement of Radon and Thoron Flux, *Radiat. Protect. Dosim.*, 67, 109–120, 1996

<sup>4</sup> Holford, D. J., Schery, S. D., Wilson, J. L., and Phillips, F. M.: Modeling Radon Transport in Dry, Cracked Soil, *J. Geophys. Res.*, 98, 567–580, doi:10.1029/92JB01845, 1993



Fig.1. View of ANSTO portable radon emanometer



Fig.2. View of accumulation chamber during radon flux measurement

The radon emanometer was calibrated at ANSTO prior to sending it to the survey site.

Most of the survey points were located outside the fence of the area of interest. The points 3 and 4 were located inside the compound on the weathered bitumen, hence their low values.

The average radon emanation values around the site is  $12 \text{ mBq m}^{-2} \text{ s}^{-1}$  and average thoron values of  $3200 \text{ mBq m}^{-2} \text{ s}^{-1}$ , which are comparable to Australian average radon emanation from soils (radon:  $23.4 \text{ mBq m}^{-2} \text{ s}^{-1}$ , thoron:  $1700 \text{ mBq m}^{-2} \text{ s}^{-1}$ )<sup>5 6</sup>.

<sup>5</sup> Schery, S., Whittlestone, S., Hart, K., and Hill, S.: The flux of radon and thoron from Australian soils, J. Geophys. Res, 94, 8567– 8576, doi:10.1029/JD094iD06p08567, 1989.

The table below summarises the measured radon emissions (May 2018):

No	Latitude	Longitude	Soil moisture %	<b>Radon</b> <b>mBq m<sup>-2</sup>s<sup>-1</sup></b>	Error mBq m <sup>-2</sup> s <sup>-1</sup>	Thoron mBq m <sup>-2</sup> s <sup>-1</sup>	Error mBq m <sup>-2</sup> s <sup>-1</sup>
1	-30.9409	136.5367	12.8	<b>15.5</b>	1.33	2641	53.8
2	-30.9409	136.5368	9.7	<b>11.4</b>	1.45	2003	48.9
3	-30.9407	136.5365	10.3	<b>4.3</b>	1.26	760	36.6
4	-30.9408	136.5364	10.7	<b>2.6</b>	1.19	1886	47.5
5	-30.9405	136.5358	7.1	<b>24.8</b>	1.69	3167	61.1
6	-30.9401	136.5361	4.1	<b>7.2</b>	1.46	4256	67.8
7	-30.9398	136.5363	5.5	<b>9.1</b>	1.29	3477	62.2
8	-30.9392	136.5368	7.4	<b>4.7</b>	1.23	4899	71.4
9	-30.9395	136.5375	2.4	<b>14.1</b>	1.45	2106	52.9
10	-30.9400	136.5382	10.3	<b>10.6</b>	1.48	2964	59.1
11	-30.9406	136.5377	1.4	<b>30.1</b>	1.67	2224	54.9
12	-30.9409	136.5375	6.6	<b>15.3</b>	1.71	3278	63.7
13	-30.9413	136.5370	3.8	<b>5.2</b>	1.71	2610	58.5
14	-30.9410	136.5364	1.9	<b>14.3</b>	1.80	2402	58.1
15	-30.9398	136.5359	5.8	<b>12.4</b>	1.88	4203	71.1
16	-30.9394	136.5354	3.3	<b>6.4</b>	1.58	2661	58.4
17	-30.9411	136.5378	10.5	<b>10.3</b>	1.63	3606	65.6
18	-30.9400	136.5354	8.8	<b>7.7</b>	1.65	4882	75.4

*Table 1. Radon emanation survey results*

<sup>6</sup> Griffiths A. D, Zahorowski W, Element A, Werczynski S. A map of radon flux at the Australian land surface. *Atmos. Chem. Phys.* 2010; 10: 8969–8982. 10.3402/tellusb.v65i0.19622.

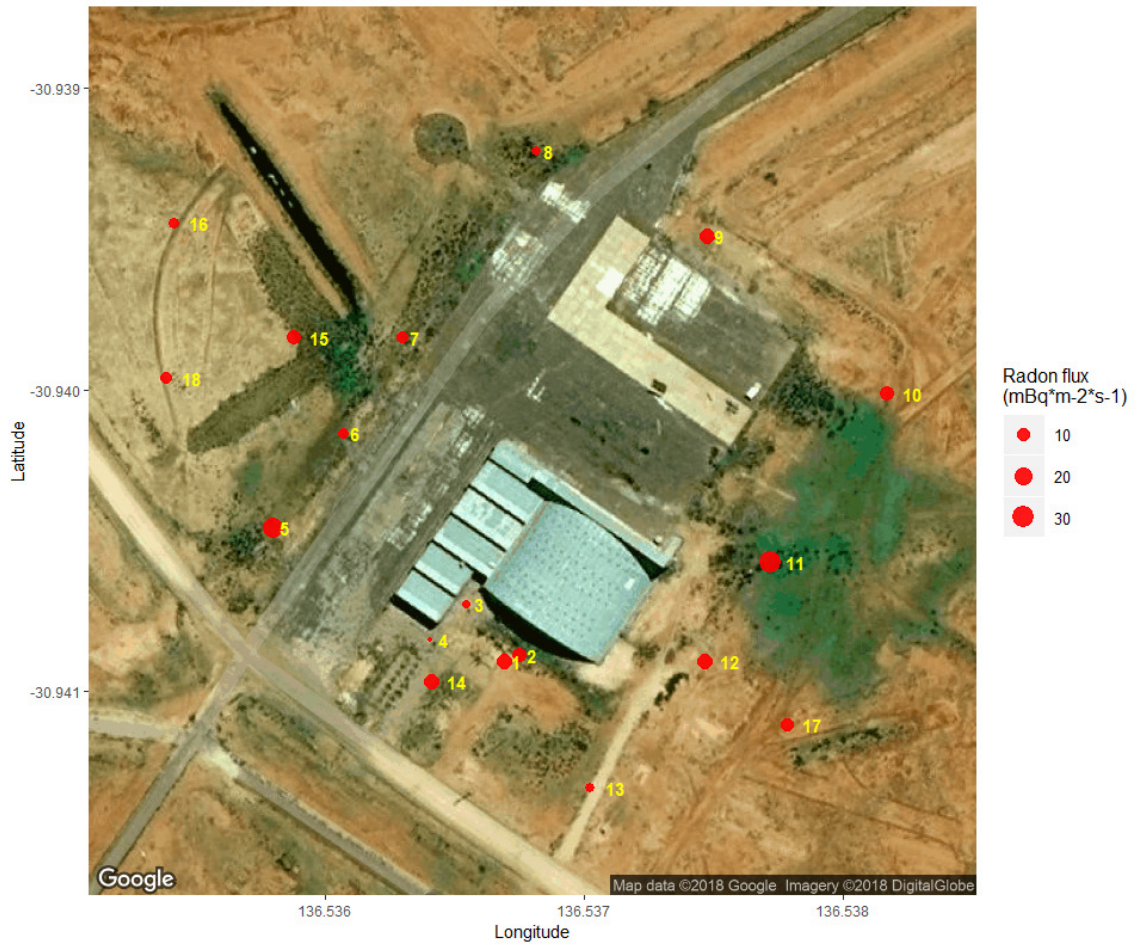


Fig.3. Radon flux survey map

### Radon in air measurements

In order to measure the <sup>222</sup>Rn concentrations in air, ANSTO continuous 100L dual-loop radon-in-air detector has been set up with AlphaGUARD portable radon monitor as a backup.

The 100L detector had been set up at the southern part of the survey area and close to the buildings at 30°56'27.9"S 136°32'13.4"E (figure 4).



Fig.4. Location of the 100L radon detector

Air sampled from an air intake mounted 2m above ground level at the rate of 18 L/min first passes through an air filter to remove dust or other aerosol pollution, as well as ambient radon progeny (products of radon's radioactive decay process) in the sampled air stream.

The air then enters the thoron delay volume (black barrel on figure 4). Thoron ( $^{220}\text{Rn}$ ) is an isotope of radon ( $^{222}\text{Rn}$ ) and can interfere with the measured radon signal. As the half-life of thoron is only 55.6 seconds, it is almost completely removed by delaying the sampled air in these thoron delay volumes by 6 minutes.

After exiting the thoron delay volume, air enters the main delay volume (metal tank on figure 5), which allows radon to decay under controlled conditions. From there the air passes through a screen, which collects the newly formed decay products. The screen sits close to a zinc sulphide scintillator, which emits light when struck by alpha particles from radon decay. The scintillator is connected to a photomultiplier tube which detects this light. This detection is processed electronically and recorded as a count rate by a data logger.

The detector was set up with solar panels charging a 12V battery, which run the instrument.

The datalogger in the 100L radon detector is also configured to continuously monitor the ambient air temperature, relative humidity, barometric pressure, and wind speed and wind direction.



Fig.5. 100L radon detector located at survey site

Due to its location, the battery for the 100L detector could not be fully charged every day, resulting in incomplete data set. Where necessary, the data from the backup portable radon monitor AlphaGUARD was used.

Three full months of radon data is available, both from the 100L detector and the backup AlphaGUARD monitor (Figure 5).

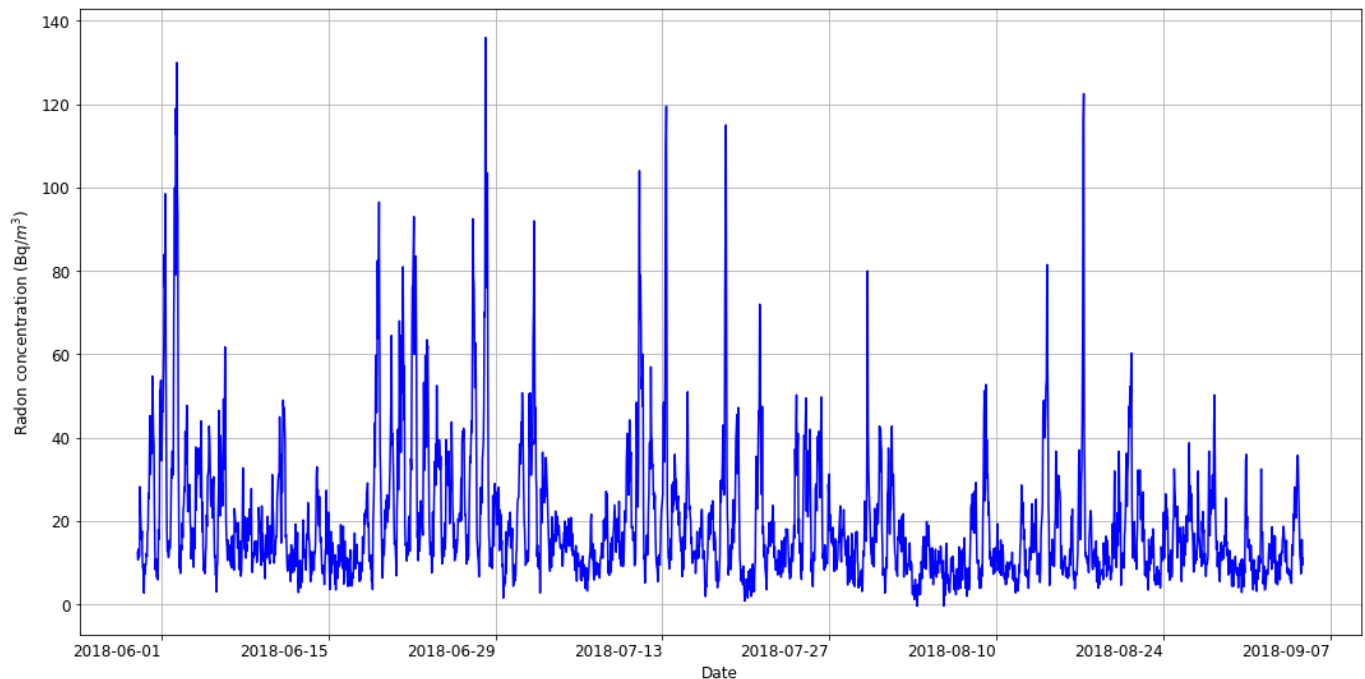


Fig.5. Hourly <sup>222</sup>Rn concentration in the air at 2 m above the ground at Woomera site

Figure 5 shows the variation of hourly outdoor radon concentration in the atmosphere for the period from June to September 2018.

Total and monthly radon concentration statistics for the site, based on a 60 min data integration period, is shown in Table 2 and Figure 6.

	Average	SD	Max
<b>All</b>	<b>19.4</b>	<b>16.0</b>	<b>136.0</b>
Jun-18	24.2	19.6	136.0
Jul-18	19.9	15.3	119.5
Aug-18	14.8	11.5	122.5

Table 2. Radon concentration statistics at the site

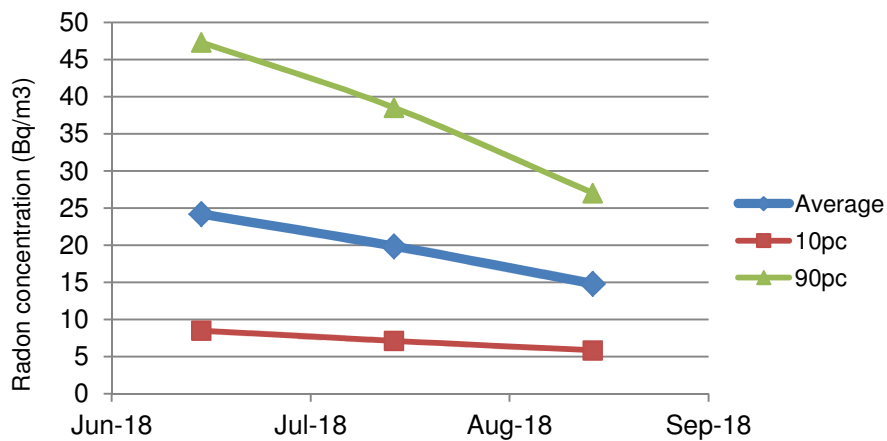


Figure 6: Monthly distributions (10<sup>th</sup> percentiles, average and 90<sup>th</sup> percentiles) of radon concentrations [Bq m<sup>-3</sup>] at the site.

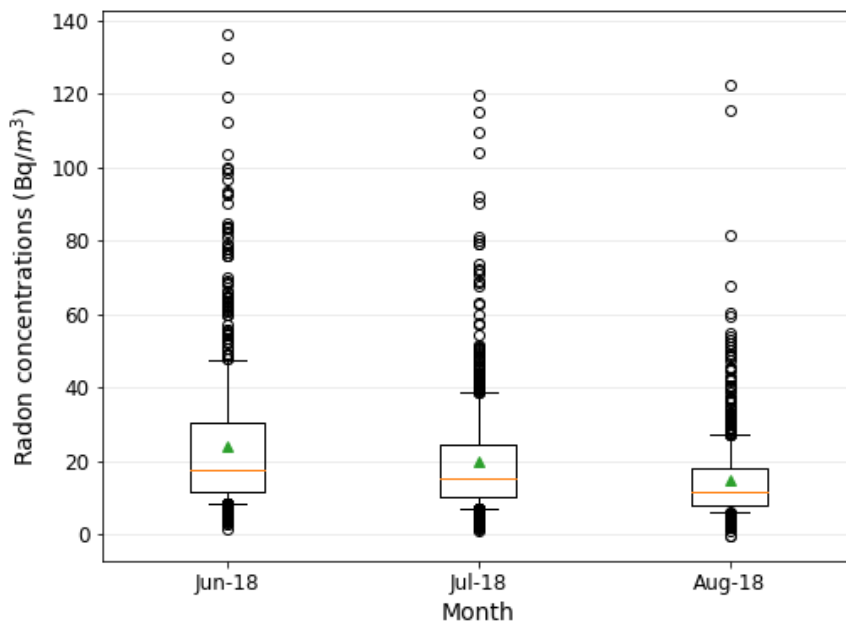


Figure 7: Monthly distributions of radon concentrations with outliers

The diurnal pattern of  $^{222}\text{Rn}$  concentration was revealed with a maximum in the early morning and a minimum in the afternoon (Fig. 8). This diurnal variation of radon concentration resulted from the formation of a surface thermal inversion at night and high turbulence in the daytime mixing layer.

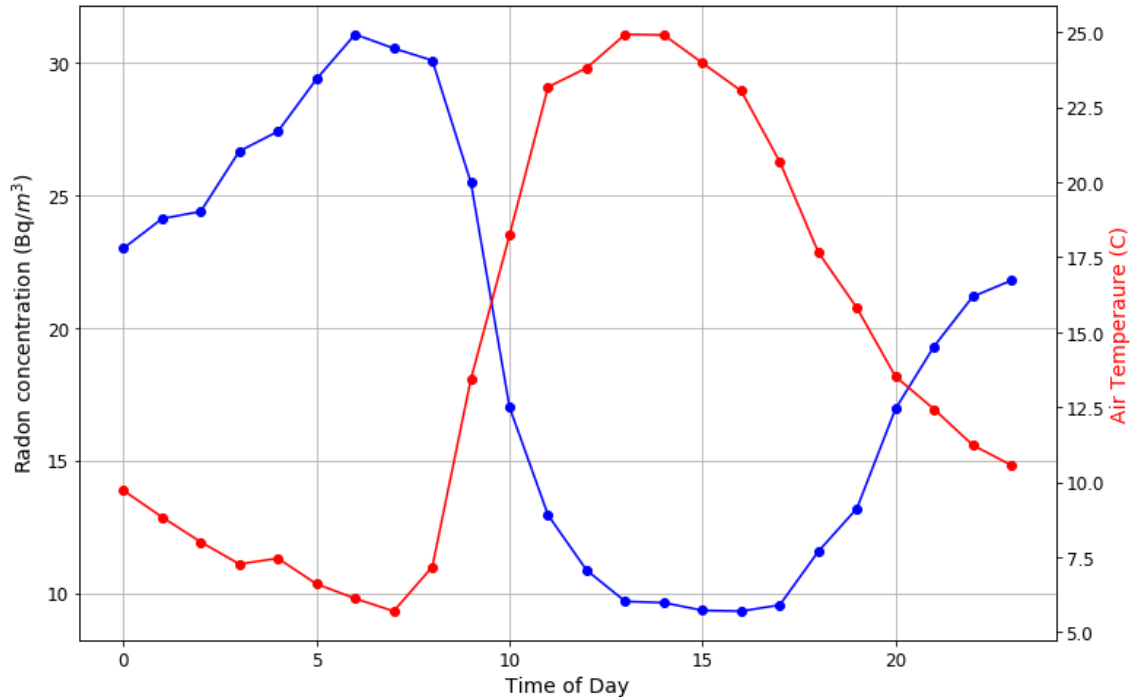


Fig.8. Mean of 24 h pattern of  $^{222}\text{Rn}$  concentration in the air and air temperature at 2 m above the ground at the site

The 100L detector is fitted with a wind speed and direction sensor (Windsonic) because of the large effect that meteorological conditions have on ambient radon concentration. In particular, the mixing height (the depth of the well-mixed layer near the ground) determines the height over which fresh radon emissions are distributed. At inland sites, the highest near-surface radon concentrations are typically seen on calm, clear nights when mixing may be limited to a few tens of metres.

The wind rose plot (Fig.9) shows the prevalent wind speed and direction at the location of 100L detector during the measurements. Although local radon emissions are relatively low, airborne radiometric surveys<sup>7</sup> indicate the potential for higher radon emissions from the westerly sector, from south west through to north east of the site<sup>8</sup>. This is confirmed on the percentile rose plot (Fig.10).

<sup>7</sup> Radiometrics map:

Radium data are taken from the Radiometric Map of Australia (Radmap 2009: Minty et al., 2009). Minty, B. R. S., Franklin, R., Milligan, P. R., Richardson, L. M., and Wilford, J.: The Radiometric Map of Australia, in: 20th International Geophysical Conference and Exhibition, Australian Society of Exploration Geophysicists, Adelaide, 2009

Radon flux data are from Griffiths et al. 2010

<sup>8</sup> "airborne radiometric surveys" are the basis of "The Radiometric Map of Australia"

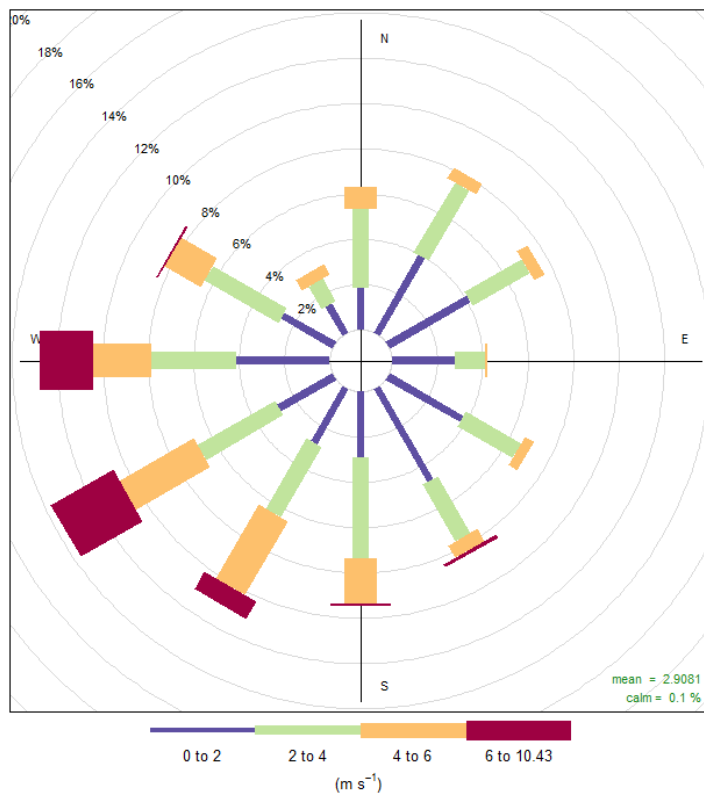


Fig.9. Wind rose plot - frequency of counts by wind direction (%)

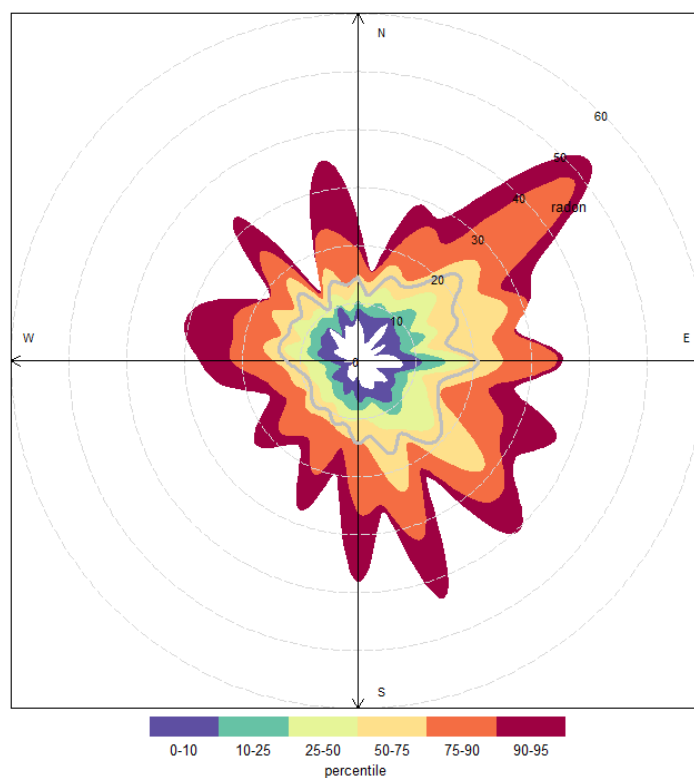


Fig.10. Percentile rose plot of radon concentrations

## Conclusions

- No measured radon concentrations at the site exceeded the recommended action levels for workplaces and dwellings<sup>9</sup>.
- Reduction in the monthly average radon concentrations at the site over the study period is likely due to stronger mixing associated with higher wind speeds and overcast conditions.
- The radon emanation from the soil at the site is comparable to Australian average radon emanation from soils.

---

<sup>9</sup> ARPANSA, 2017: Radiation Protection Series G-2, Guide for Radiation Protection in Existing Exposure Situations (September 2017), Annex A. Available at: <https://www.arpansa.gov.au/regulation-and-licensing/regulatory-publications/radiation-protection-series/guides-and-recommendations/rpsg-2>